Real-Time Adaptive Control of Flow-Induced Cavity Tones (Invited)

Michael A. Kegerise* and Randolph H. Cabell†
NASA Langley Research Center, Hampton, VA 23681

Louis N. Cattafesta‡
University of Florida, Gainesville, FL 32611

An adaptive generalized predictive control (GPC) algorithm was formulated and applied to the cavity flow-tone problem. The algorithm employs gradient descent to update the GPC coefficients at each time step. The adaptive control algorithm demonstrated multiple Rossiter mode suppression at fixed Mach numbers ranging from 0.275 to 0.38. The algorithm was also able to maintain suppression of multiple cavity tones as the freestream Mach number was varied over a modest range (0.275 to 0.29). Controller performance was evaluated with a measure of output disturbance rejection and an input sensitivity transfer function. The results suggest that disturbances entering the cavity flow are colocated with the control input at the cavity leading edge. In that case, only tonal components of the cavity wall-pressure fluctuations can be suppressed and arbitrary broadband pressure reduction is not possible. In the control-algorithm development, the cavity dynamics are treated as linear and time invariant (LTI) for a fixed Mach number. The experimental results lend support this treatment.

Introduction

THE grazing flow over a cavity is characterized by a complex feedback process that leads to large-amplitude acoustic tones. Instability waves in the cavity shear layer grow and convect downstream. The resulting unsteady shear-layer impingement on the downstream corner acts as a noise source. Sound from this source propagates upstream to the cavity leading edge. Here, the feedback disturbances are converted to instability waves through a receptivity process to complete the feedback loop. A schematic illustrating the physical elements of the cavity-tone process is shown in Fig. 1. Cavity flow-tone generation is of practical concern to several engineering applications. In aircraft weapons bays, for example, the high sound pressure levels (~ 160 *dB re* $20\mu Pa$) associated with the tones can be damaging to stores within the bay and can influence the trajectory of released stores.[1]

Passive and open-loop active control methodologies were employed for the suppression of cavity-flow tones in past studies. Feedback flow control, however, has only recently been applied to the problem.[2–8] An overview of the various feedback-control methodologies used is given in the review paper by Cattafesta

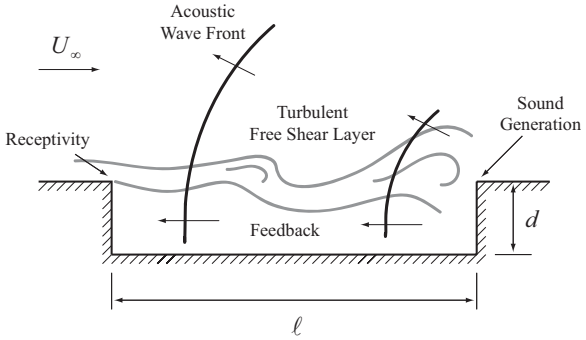

Fig. 1 Schematic illustrating the physical elements of flow-induced cavity tones.

et al.[9] There are particular benefits to this approach over passive or open-loop control methods. Reduced energy consumption,[6] no drag penalty, and robustness to parameter changes and modeling uncertainties are among these benefits. Feedback control algorithms can also be made to adapt to changes in process dynamics that are brought about by changes in freestream conditions.

Aside from the practical interest, the cavity flow problem is an excellent test bed for real-time, closed-loop flow control. Here, real-time implies that the control effort is computed at the sample rate of a digital controller. Although the geometry is relatively simple and the physics is low dimensional in the sense that only a small number of narrowband tones are to be suppressed, the physics of the process is both rich and complex. The multiple tones, or Rossiter modes,[11] often experience significant nonlinear coupling and mode switching,[12,13] the dynamics of the process are sensi-

*Research Scientist, Flow Physics and Control Branch. Member AIAA.

†Research Scientist, Structural Acoustics Branch. Member AIAA.

‡Associate Professor. Associate Fellow AIAA.

Copyright © 2004 by the American Institute of Aeronautics and Astronautics, Inc. No copyright is asserted in the United States under Title 17, U.S. Code. The U.S. Government has a royalty-free license to exercise all rights under the copyright claimed herein for Governmental Purposes. All other rights are reserved by the copyright owner.

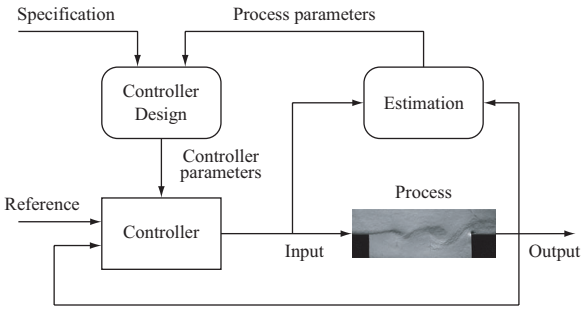

Fig. 2 Block diagram of a self-tuning adaptive controller (after Astrom and Wittenmark[14]).

tive to freestream Mach number, and there are convective delays between control inputs and sensor outputs. These physical elements are present in many other active flow-control problems. It is expected therefore that control algorithms and approaches developed for this problem will find broader application. Most importantly, the required sensors, actuators, and digital signal processing (DSP) hardware are at a mature enough level such that real-time adaptive control of flow-induced cavity tones is currently feasible.

The present interest is in the development of a self-tuning adaptive controller for cavity tone suppression. The elements of this controller are shown in Fig. 2. There are two distinct loops in the adaptive controller. The inner loop is a dynamic feedback control system comprised of the process and controller. In this loop, the controller operates at a sample rate that is suitable for the process under control. The output is unsteady pressures at the cavity walls. The reference signal is set to zero since the control objective is to minimize the output. The outer loop consists of the model estimation and controller design steps. Model estimation refers to the identification of a model from process input-output data. The identified process parameters and a specified cost function are then used to design a controller that will minimize the output pressures. Both steps can be performed recursively at the sample rate of the controller (*i.e.,* in real time) or they can be performed off-line in a batch mode. This choice depends on whether the plant is time varying or time invariant. Pillarisetti and Cattafesta[10] and Kegerise *et al.*[4] have presented algorithms that are suitable for the recursive identification of a process model for the cavity flow. Cabell *et al.*[5] used a batch-mode approach to obtain fixed-gain control laws that were suitable only for the Mach numbers at which they were designed.

This paper presents the development and application of a recursive controller design algorithm for eventual use in a self-tuning adaptive controller. Specifically, a gradient descent algorithm was used to adaptively tune the controller parameters at each time step while the process parameters were held constant. The gradient descent procedure is an efficient method for tuning the controller parameters, and is seen as an important step towards enabling fully adaptive control of cavity tones.

The paper is organized as follows. The control methodology and algorithm are presented in the next section. This is followed by a description of the experimental setup and data processing methods. The results of the control experiments are then presented and discussed. In the discussion, the performance limitations and the transient behavior of the control algorithm are considered. Finally, results demonstrating controller adaption to changing freestream Mach number are presented.

Control Methodology

In the feedback control of cavity-flow tones, the objective is to minimize the output fluctuating pressure on the cavity walls. This is disturbance rejection in controls terminology. The output sensors are pressure transducers embedded in the cavity walls and they serve as both feedback signals and as performance measures. The control input is provided by an actuator situated at the cavity leading edge. A piezoelectric flap-type actuator was used in the present study. Physically, the controller attempts to cancel the instability waves in the cavity shear layer that result from the aeroacoustic feedback loop. This, in turn, results in an unsteady pressure reduction at the output sensors.

There are several control-design methods that can be used to meet the objective. The particular control law used in this study is the generalized predictive controller (GPC). The GPC is based on a finite range prediction equation for future plant outputs. A cost function is then defined and subsequently minimized to determine the controller coefficients. The GPC was first introduced by Clarke *et al.*[20,21] and has since been successfully applied to many active vibration and noise control problems. It is applicable to plants that are non-minimum phase, plants that are open-loop unstable or have lightly-damped poles and plants that have delays. Since the cavity flow dynamics exhibit several of these features, the GPC was considered to be a good candidate for the problem.

As with many control-design approaches, a mathematical model of the process must be available for controller design. While a physics-based model is desirable, none of sufficient accuracy is currently available. Instead, an empirical model, whose parameters are determined from input-output data, can be used. This is referred to as system identification.

System Identification

The model structure chosen to represent the cavity-flow dynamics was a discrete-time linear model given by:

$$\begin{aligned} y(k) &= \alpha_1 y(k-1) + \ldots + \alpha_p y(k-p) \\ &\quad + \beta_0 u(k) + \ldots + \beta_p u(k-p), \end{aligned} \tag{1}$$

where $y(k)$ are the $m \times 1$ outputs, $u(k)$ are the $r \times 1$ inputs, p is the model order, and k is the current time step. This model structure is commonly referred to as an ARX (auto-regressive, exogenous input) model.[15,16] The coefficient matrices, α_i $(i = 1, 2, \ldots, p)$ of $m \times m$ and β_i $(i = 0, 1, 2, \ldots, p)$ of $m \times r$, are the ARX parameters or the observer Markov parameters.

To determine the observer Markov parameters of the model, the observer/Kalman filter identification (OKID) algorithm of Juang *et al.*[15,18,19] was used. The input to the algorithm is experimental input-output data from the open-loop plant. To obtain this data, the actuator was driven with a broadband signal and input-output time-series data were collected. Models were identified for each of the flow conditions considered in the control experiments.

Adaptive GPC Algorithm

The algorithm development begins with a predictive matrix equation formed from the ARX model:[18,19,22,23]

$$\mathbf{y}_s(k) = \mathbf{T}\mathbf{u}_s(k) + \mathbf{\Theta}\mathbf{v}_p(k-p), \tag{2}$$

where $\mathbf{y}_s(k)$ is a $sm \times 1$ vector of current and future outputs:

$$\mathbf{y}_s(k) = \left\{ \begin{array}{c} y(k) \\ y(k+1) \\ \vdots \\ y(k+s-1) \end{array} \right\}, \tag{3}$$

$\mathbf{u}_s(k)$ is a $sr \times 1$ vector of current and future inputs:

$$\mathbf{u}_s(k) = \left\{ \begin{array}{c} u(k) \\ u(k+1) \\ \vdots \\ u(k+s-1) \end{array} \right\}, \tag{4}$$

and $\mathbf{v}_p(k-p)$ is a $p(m+r) \times 1$ vector of past inputs and outputs running from time step $k-p$ to $k-1$:

$$\mathbf{v}_p(k-p) = \left\{ \begin{array}{c} u(k-p) \\ \vdots \\ u(k-1) \\ y(k-p) \\ \vdots \\ y(k-1) \end{array} \right\}. \tag{5}$$

The parameter s is referred to as the prediction horizon. The predictive matrix equation states that the future output data depends on the future control inputs and past input-output data. The matrix $\mathbf{T}$ is an $sm \times sr$ Toeplitz matrix:

$$\mathbf{T} = \left[\begin{array}{ccccc} \beta_0 & & & & \\ \beta_0^{(1)} & \beta_0 & & & \\ \beta_0^{(2)} & \beta_0^{(1)} & \beta_0 & & \\ \vdots & \vdots & \ddots & \ddots & \\ \beta_0^{(s-1)} & \beta_0^{(s-2)} & \cdots & \beta_0^{(1)} & \beta_0 \end{array} \right] \tag{6}$$

where $\beta_0, \beta_0^{(1)}, \cdots, \beta_0^{(s-1)}$ are the pulse response parameters of the open loop plant. These parameters can be obtained from the observer Markov parameters.[18] The rectangular matrix $\mathbf{\Theta}$ is formed with a set of recursive equations and the ARX parameters.[18] As will be shown below, however, this matrix is not needed in the real-time implementation.

The control input is computed as:

$$\mathbf{u}_s(k) = \mathbf{H}\mathbf{v}_p(k-p), \tag{7}$$

where $\mathbf{H}$ denotes the $sr \times p(m+r)$ matrix of controller coefficients.

The next step in the algorithm development is to define a cost function:

$$J = \mathbf{y}_s^T(k)\mathbf{Q}\mathbf{y}_s(k) + \gamma \cdot tr\left(\mathbf{H}^T\mathbf{H}\right), \tag{8}$$

where J is a scalar value and $tr\,(\cdot)$ denotes the trace of the matrix in parentheses. The first term in Eq. 8 is the sum of the squared output values over the prediction horizon and $\mathbf{Q}$ is a $sm \times sm$ block-diagonal matrix of sensor weights:

$$\mathbf{Q} = \left[\begin{array}{ccc} q & 0 & 0 \\ 0 & \ddots & 0 \\ 0 & 0 & q \end{array} \right] \tag{9}$$

where the submatrix q is a $m \times m$ diagonal matrix of sensor weights:

$$q = \left[\begin{array}{ccc} q_1 & 0 & 0 \\ 0 & \ddots & 0 \\ 0 & 0 & q_m \end{array} \right]. \tag{10}$$

The sensor weights $q_1, \cdots, q_m$ take on values between 0 and 1. A value of zero means that the sensor is not included in the cost function, but the sensor information is still used by the feedback controller.

The second term in the cost function imposes an effort penalty on the control input. This term is necessary to avoid large control inputs and actuator saturation. It has other benefits that will be discussed below.

The present goal is to determine the controller coefficients, $\mathbf{H}$, such that the cost function is minimized. One way, that is computationally efficient, is to use a stochastic gradient-descent algorithm that iteratively

searches the performance surface, $J(\mathbf{H})$, for the optimal value. This algorithm updates the controller coefficients at each time step with:

$$\mathbf{H}(k+1) = \mathbf{H}(k) - \mu \frac{\partial J(k)}{\partial \mathbf{H}}, \tag{11}$$

where the gradient of J is an instantaneous or stochastic estimate and μ sets the adaptive rate of the algorithm. This equation is the basis for the well known least-mean squares (LMS) algorithm.[24,25]

The gradient of the cost function can be determined by substituting Eqs. 2 and 7 into Eq. 8 and taking the derivative with respect to $\mathbf{H}$. After some algebraic manipulation:

$$\frac{\partial J(k)}{\partial \mathbf{H}} = 2\mathbf{T}^T\mathbf{Q}\mathbf{y}_s(k)\mathbf{v}_p^T(k-p) + 2\gamma\mathbf{H}(k). \tag{12}$$

Substituting this expression into Eq. 11 gives:

$$\mathbf{H}(k+1) = \alpha\mathbf{H}(k) - 2\mu\mathbf{T}^T\mathbf{Q}\mathbf{y}_s(k)\mathbf{v}_p^T(k-p) \tag{13}$$

where $\alpha = (1-2\mu\gamma)$. Examination of the update equation indicates that it depends on future input values, $\mathbf{u}_s(k)$, and future output values, $\mathbf{y}_s(k)$, and so cannot be implemented in real time. However, assuming the gradient of the cost function does not change significantly over the prediction horizon, s, the data vectors can be shifted back in time by s time steps and the update equation becomes:

$$\begin{aligned}\mathbf{H}(k+1) &= \alpha\mathbf{H}(k) \\ &\quad -2\mu\mathbf{T}^T\mathbf{Q}\mathbf{y}_s(k-s)\mathbf{v}_p^T(k-p-s).\end{aligned} \tag{14}$$

The variable α in the update equation is referred to as the leakage factor. It arises from the $\gamma \cdot tr(\mathbf{H}^T\mathbf{H})$ term in the cost function.[24,26,27] The value of α is typically set to slightly less than one (*e.g.*, $\alpha = 0.9999$). In that case, the controller coefficients come close to, but never reach, their optimal values. Instead, they constantly fluctuate in a region about their optimal values. The benefits of leakage in the update equation include improved robustness and rate of convergence.[24,25,27] Leakage also counteracts parameter drift that can occur in the standard LMS algorithm.[24] Most importantly, leakage acts like an effort penalty on the control input.[26,27]

The control law in Eq. 7 yields a vector of current and future inputs. In the real-time implementation of this control law, however, the current control effort, $u(k)$, is applied to the process and the future values are discarded at each time step. Therefore, it is sufficient to compute the current control effort as:

$$u(k) = \mathbf{h}\mathbf{v}_p(k-p), \tag{15}$$

where $\mathbf{h}$ denotes the first r rows of the matrix $\mathbf{H}$. In turn, the update equation can be rewritten to update the $r \times p(m+r)$ matrix $\mathbf{h}$ as:

$$\begin{aligned}\mathbf{h}(k+1) &= \alpha\mathbf{h}(k) \\ &\quad -2\mu\left\{\mathbf{T}^T\mathbf{Q}\right\}_r\mathbf{y}_s(k-s)\mathbf{v}_p^T(k-p-s),\end{aligned} \tag{16}$$

where the subscript r denotes the first r rows of the matrix $\mathbf{T}^T\mathbf{Q}$.

To implement the adaptive GPC algorithm in real time, the required algorithm steps are:

1. Determine the ARX parameters via system identification and form the matrix, $\left\{\mathbf{T}^T\mathbf{Q}\right\}_r$.
2. Initialize $\mathbf{h}(0)$ to zero.
3. Update the data vectors $\mathbf{y}_s(k-s)$ and $\mathbf{v}_p(k-p-s)$.
4. Update $\mathbf{h}(k)$ according to Eq. 16.
5. Compute the control effort as: $u(k) = \mathbf{h}\mathbf{v}_p(k-p)$.
6. Repeat steps 3 to 5.

In the algorithm listing above, it is assumed that the system to be controlled is linear and time invariant. In that case, the system identification can be performed offline in a batch mode before running the control algorithm. Also, it is expected that the controller coefficients will converge to a steady-state level. In our control approach, the cavity dynamics are treated as linear and time invariant for a *fixed* Mach number. Therefore, the system identification was performed offline for each of the Mach numbers tested. Whether this is a reasonable approach to the problem will be discussed in the results section. It is important to recognize, however, that system identification will have to be performed recursively to track changes in the cavity dynamics that result from a change in the freestream conditions.

There are several parameters in the algorithm that must be tuned to achieve a balance between optimal performance and stability of the controller: the model order p, the prediction horizon s, the adaptive rate μ, the leakage factor α, and the sampling rate. Although the parameter values are problem dependent, experience provides some guidelines for their selection. The model order is selected through system identification. The key issue in this case is to chose p large enough such that all of the pertinent open-loop dynamics are captured by the model. The prediction horizon should be at least equal to the model order, but in practice, is typically taken as 2 to 3 times the model order.[22] For the sampling rate, experience indicates that a value 2 to 3 times the highest frequency results in the best performance.[22] The highest frequency in the present context is the highest Rossiter frequency of interest.

The parameter μ controls the convergence rate of the algorithm. As the value of μ is increased, the convergence time of the algorithm decreases, but for too

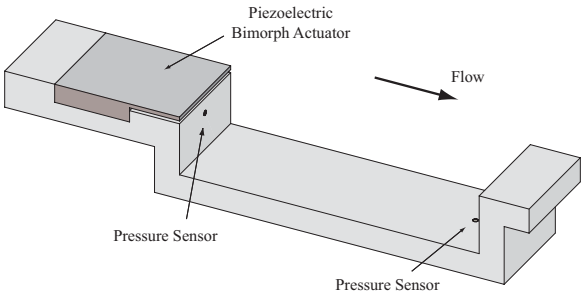

Fig. 3 Schematic of cavity model showing sensor and actuator locations.

large a value, the algorithm will become unstable. Ideally, μ should be chosen such the convergence time of the algorithm is smaller than the time scale over which the process dynamics change.

As mentioned above, the numerical value of α is typically slightly less than one. As the leakage factor approaches one, the control effort penalty decreases, resulting in a more aggressive controller. It is important to recall that α also depends on μ; *i.e.,* $\alpha = 1 - 2\mu\gamma$. For example, if μ is decreased but α remains the same, the implication is that γ has increased. A larger value of γ results in a larger control-effort penalty and therefore, a more sluggish, stable controller. The upshot of this interdependence is μ and α must both be tuned to achieve a balance between the optimal performance, convergence rate, and algorithm stability.

Experimental Details

The details of the experimental setup and data processing methods are presented in this section.

Wind Tunnel Facility

The experimental program was conducted in the NASA-Langley Probe Calibration Tunnel (PCT). The PCT is typically operated as an open-jet pressure tunnel with independent control of stagnation pressure, stagnation temperature, and freestream velocity. For the current experiment, the facility was fitted with a subsonic nozzle that contracts from a circular inlet to a 50.8 *mm* by 152.4 *mm* exit. A straight duct section of length 0.6 *m* was attached to the nozzle exit and was terminated with a small-angle diffuser. The freestream Mach number range for the present tunnel configuration was 0.04 to 0.8.

Cavity Model

A rectangular cavity model was installed in the ceiling of the straight duct section of the PCT. The floor of the duct section was a foam filled baffle that minimized reflections of acoustic waves radiated by the cavity. The cavity model had a fixed length, $\ell = 152.4$ *mm*, and a variable depth, d, which was fixed to 30.48 *mm* for an ℓ/d ratio of 5. The cavity model spanned the width of the test section ($w = 50.89$ *mm*) to provide an un-obscured view of the cavity shear layer for optical diagnostics. The incoming boundary layer was

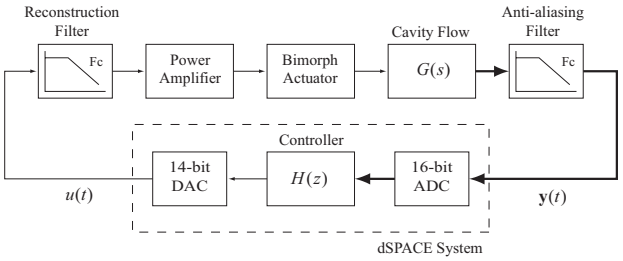

Fig. 4 Block diagram of feedback control system.

turbulent with a thickness of approximately 6 *mm*. A schematic of the cavity is shown in Fig. 3.

Actuator

The actuator for the present study was a piezoelectric bimorph cantilever beam with its tip situated at the cavity leading edge (Fig. 3). This actuator was chosen for its relatively high bandwidth ($\sim$ 1 *kHz*) and ability to generate large streamwise disturbances with modest tip deflections (on the order of tens of micrometers[4, 28]). The response of the actuator was characteristic of a 2nd-order underdamped system with a natural frequency of $\approx$ 1200 *Hz* and a DC gain of ≈ 0.25 $\mu m/V$. Further details on the design and construction of the actuator can be found in Kegerise *et al.*,[4] Mathew[29] and Schaeffler *et al.*[30]

Sensors

The cavity model was instrumented with a pair of piezoresistive pressure transducers. The nominal sensitivity and bandwidth of the sensors were 2.2×10^{-5} *V/Pa* and 14 *kHz*, respectively. One sensor was located in the midplane of the front cavity wall, 12 *mm* down from the cavity leading edge. The second sensor was located in the floor midplane, 15 *mm* upstream from the cavity rear wall (see Fig. 3).

Control Hardware

A block diagram of the feedback control setup is shown in Fig. 4. The voltage signals from the pressure sensors were first pre-amplified and anti-aliased filtered. The filters were 6th-order (6-pole/6-zero) with nearly constant group delay (linear phase) in the passband. The zero-frequency group delay was $0.715/F_c$ *sec* and the cutoff frequency was $F_c = 1600$ *Hz*. The signals were then sampled with a 16-bit A/D.

The control algorithm was coded in SIMULINK and then converted to compiled code via Real-Time Workshop to run on a floating-point DSP (dSPACE DS1005 card with a clock speed of 480 *MHz*). Based on the current and past sampled voltages from the pressure sensors and past control efforts, the control algorithm computed the control signal once per time step. For all of the results presented in this paper, the sample time of controller was set to 250 μsec.

The computed control effort was then converted to an analog signal via a 14-bit D/A card. This signal was passed to a reconstruction filter (same type as

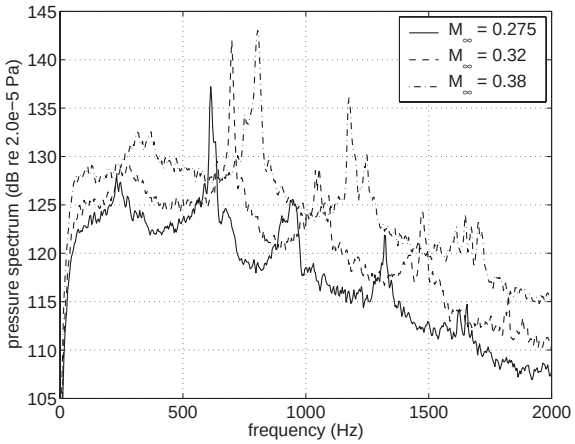

Fig. 5 Baseline pressure spectra of rear-floor sensor. $\ell/d = 5$**.**

anti-alias filter with $F_c = 1600$ *Hz*) to smooth the zero-order hold signal from the D/A card. The output of this filter was sent to a high-voltage amplifier to produce the drive signal for the bimorph actuator.

Data Processing

Pressure sensor time-series data were collected for both the baseline (open-loop) and controlled cavity flow. Primarily, the data were processed to obtain pressure spectra. In computing the spectra, 1024 point FFTs, a hanning window, 50% overlap, and 160 block averages were used. The sample rate for data collection was 4 *kHz* and the frequency resolution of the spectra was 3.9 *Hz*. The pressure spectra are presented in the results section as *dB re* 2.0×10^{-5} *Pa*.

Results and Discussion

The results of the control experiments are presented in this section. Three freestream Mach numbers were considered: $M_\infty = 0.275$, 0.32, and 0.38. Throughout the tests, the cavity geometry was fixed to $\ell/d = 5$, the total pressure was 138 *kPa*, and the total temperature was 297 *K*. The Reynolds number based on cavity length ($Re_\ell = \ell U_\infty/\nu$) for the three test conditions ranged from 1.2×10^6 to 1.6×10^6.

The section begins with a discussion of the baseline flow for the three test conditions. A series of control results for the test cases are then presented and performance limitations are discussed. This is followed by an examination of the transient behavior of the adaptive GPC algorithm at fixed Mach numbers. The section ends with a demonstration of controller adaptation to changing freestream Mach number.

Baseline Flow

Baseline pressure spectra for the three test conditions are presented in Fig. 5. The spectra display the characteristic multiple resonant tones that increase in frequency with increasing Mach number. The tone amplitudes and broadband levels also increase with increasing Mach number. Peaks in the pressure spectrum that correspond to Rossiter modes were identified from the coherence function between the two sensors in the cavity. The frequencies of these peaks were compared to those obtained from the modified Rossiter equation:[31]

$$St_\infty = \frac{m_{st} - \alpha_{st}}{M_\infty \left(1 + \frac{\gamma-1}{2} M_\infty^2\right)^{-1/2} + 1/k_{st}}, \qquad (17)$$

where $St_\infty = f\ell/U_\infty$ is the Strouhal number, m_{st} is the (integer) mode number, and $\alpha_{st} = 0.25$ and $k_{st} = 0.66$ are empirical constants. The results are presented in Table 1. The agreement is within 10%, verifying that the present cavity model behaves as expected.

Adaptive GPC Results

The adaptive GPC algorithm was applied to the three Mach-number conditions. For each of the flow conditions, control runs for a range of algorithm parameters were performed. In each case, the initial conditions were set to zero and the algorithm was used to adapt the controller coefficients over a period of time. It was found that the controller coefficients converged to steady-state levels in the mean. However, the controller coefficients do exhibit stochastic fluctuations about these mean levels. Once the controller coefficients converged, time series of the unsteady wall pressures were collected and pressure spectra were computed. For any given set of control parameters and a given Mach number, the control algorithm was run several times. Each time, the controlled pressure spectra were repeatable, suggesting that the controller coefficients were converging to the same set of values. Comparison of the controller coefficients for the several runs revealed that this was indeed true.

Control results for the three Mach number conditions are presented in Figs. 6a, c, and e. The figures show baseline and controlled pressure spectra measured at the rear-floor sensor. These results are representative of the best performance achieved for each flow condition. Multiple Rossiter modes were suppressed by the control algorithm at all three conditions. For the $M_\infty = 0.275$ case in particular, the first four Rossiter modes exhibit some suppression. The broadband levels of the pressure fluctuations are not significantly altered in any of the control runs.

Table 2 lists the algorithm parameters for the results shown in Fig. 6. For all cases, the model order used in system identification was 80 and the prediction horizon was set to 240. The sensor weights for the two outputs were zero for the front sensor (q_1) and one for the rear sensor (q_2). The control performance was found to be weakly dependent on the sensor weights, and only subtle differences were observed with different values of sensor weightings. At each flow condition the convergence rate, μ, and leakage parameter, α, were adjusted

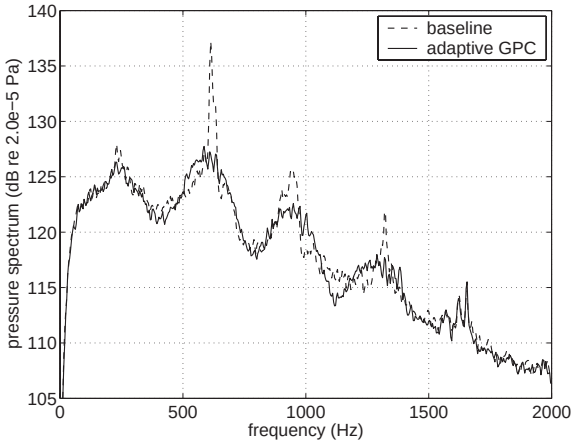

a) Baseline and controlled pressure spectra measured at rear-floor sensor. $M_\infty = 0.275$.

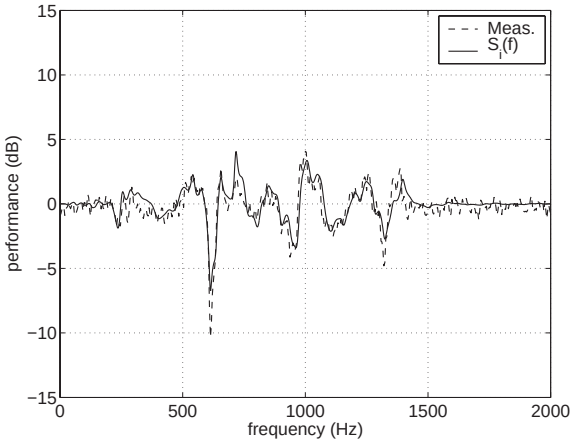

b) Measured performance and input sensitivity for adaptive GPC. $M_\infty = 0.275$.

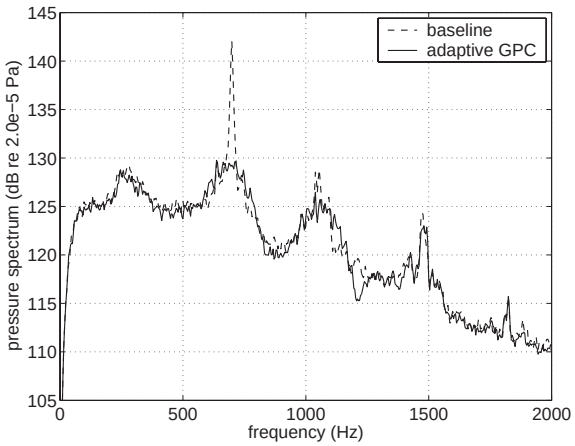

c) Baseline and controlled pressure spectra measured at rear-floor sensor. $M_\infty = 0.32$.

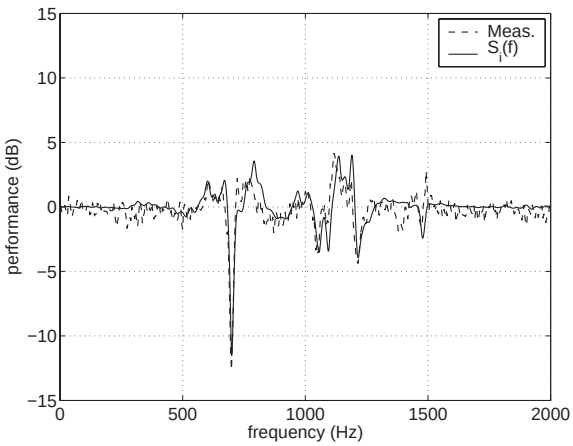

d) Measured performance and input sensitivity for adaptive GPC. $M_\infty = 0.32$.

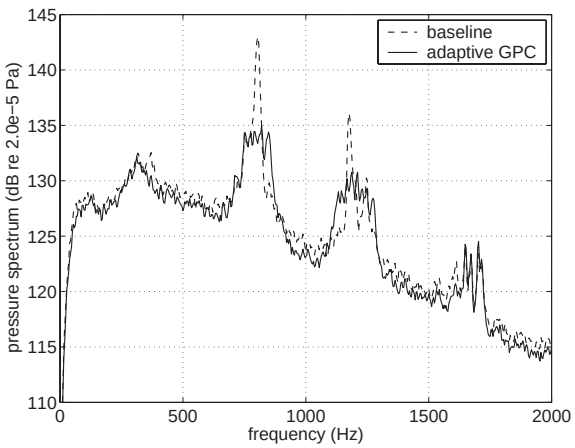

e) Baseline and controlled pressure spectra measured at rear-floor sensor. $M_\infty = 0.38$.

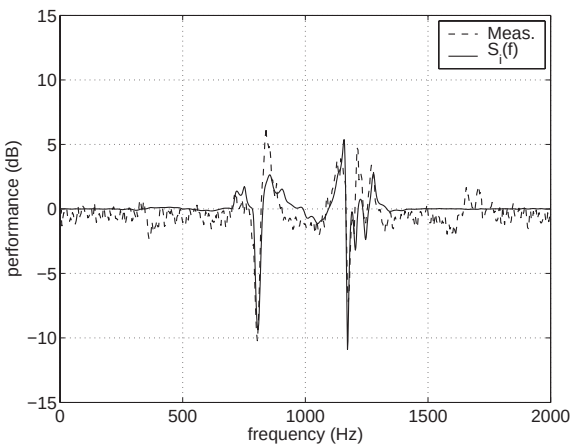

f) Measured performance and input sensitivity for adaptive GPC. $M_\infty = 0.38$.

Fig. 6 Adaptive GPC control results at three Mach numbers.

Table 1 Measured vs. predicted frequencies (Hz) of the first 4 Rossiter modes

	Mode 1		Mode 2		Mode 3		Mode 4	
M_∞	Meas.	Pred.	Meas.	Pred.	Meas.	Pred.	Meas.	Pred.
0.275	240	260	613	605	945	952	1320	1298
0.32	280	295	699	688	1054	1081	1475	1474
0.38	312	339	806	792	1175	1244	1650	1696

Table 2 Algorithm parameters

	Model Order	Pred. Horizon	Sensor Weights		Leakage Factor	Adaptive Rate
M_∞	p	s	q_1	q_2	α	μ
0.275	80	240	0	1	0.999995	0.0001
0.32	80	240	0	1	0.99999	0.00001
0.38	80	240	0	1	0.999999	0.000001

to achieve the best performance while maintaining stability and avoiding actuator saturation.

Performance Limitations

In previous feedback control studies of cavity-flow tones, several performance limitations were noted. Specifically, the controllers excited new tones or side bands of the Rossiter modes.[5,32] The latter phenomenon is referred to as peak splitting. None of the previous studies reported significant reductions in the broadband pressure fluctuations. In the present control experiments, the excitation of new tones was not observed. While the pressure spectra do not indicate distinct peak splitting, a close examination of the controlled pressure spectra reveals increased energy in frequency bands around the Rossiter modes. This behavior, which is common in the feedback control of sound and vibration, is referred to as spillover. It follows from the definition of Hong and Bernstein[34] which states that spillover occurs at frequency f when the closed-loop transfer-function magnitude is greater than the open-loop transfer function magnitude at that frequency. The result is disturbance amplification in the output sensors.

A performance measure can be defined to better represent the spillover observed in the control results:

$$\frac{\|\mathbf{y}_{cl}(f)\|_2}{\|\mathbf{y}_{ol}(f)\|_2}, \tag{18}$$

where $\mathbf{y}_{cl}$ and $\mathbf{y}_{ol}$ are vectors of the output sensor spectra for the controlled and baseline cases, respectively, and $\|\cdot\|_2$ is the 2-norm. Eq. 18 essentially provides a scalar measure of disturbance rejection for the multiple output sensors. A value less than one indicates disturbance attenuation, while a value greater then one indicates disturbance amplification. The performance measure was calculated for each of the control cases and the results are indicated by the dashed lines in Figs. 6b, d, and f. As expected, the performance measure is less than one (negative log magnitude) at the Rossiter modes where attenuation has occured, but this is always accompanied by amplification (positive log magnitude) in sideband frequencies.

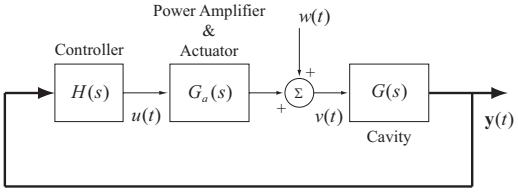

Fig. 7 SIMO model of the cavity and controller.

To understand why spillover arises in the feedback control results, the definition of a sensitivity transfer function is useful. The sensitivity was recently used by Rowley *et al.*[32] to explain performance limitations in the feedback control of cavity tones. Consider the single-input/multiple-output (SIMO) model for the cavity-flow control system shown in Fig. 7. The thicker lines indicate multidimensional signals, while the thinner lines indicate scalar signals. The disturbance, $w(t)$, is hypothesized to enter the system at the cavity leading edge, where the shear layer is especially receptive to inputs. The disturbance is subsequently filtered by the cavity dynamics before reaching the output sensors. In the absence of feedback control, this disturbance drives the response in the output sensors. This viewpoint, that cavity-flow oscillations can be described as forced oscillations of a lightly-damped, linear system, was recently put forth by Rowley *et al.*[32,33]

The control input is hypothesized to follow the same path to the output sensors as the disturbance, as indicated in Fig. 7. With this hypothesis, anything the controller does to reject the disturbance will be reflected equally in all output sensors.

The input sensitivity for this SISO system can be used to verify this hypothesis. The input sensitivity represents the transfer function between the disturbance, $w(t)$, and the plant input, $v(t)$, and is written as:

$$S_i = \frac{1}{1 - \mathbf{HP}}, \tag{19}$$

where $\mathbf{P} = \mathbf{G}G_a$ is the plant transfer function and $\mathbf{H}$ is the controller transfer function. For a SIMO system with a single disturbance following the same path to the error sensors as the control input, the input sensitivity can be shown to be equal to the performance measure defined in Eq. 18. The mathematical details of this equality are presented in the appendix. If the disturbance follows another path or if there are multiple disturbance paths to the output sensors, then this will not be true.

The log magnitude of the input sensitivity ($20 \log(|S_i|)$) is indicated by the solid line in Figs. 6b, d, and f. The good agreement between the input sensitivity and the measured performance for the $M_\infty = 0.275$ case supports the above hypothesis that the disturbance enter the system at the input. As the Mach number is increased, however, the differences between them increase. These differences can arise from uncertainties in the plant model used to calculate S_i and other disturbances that follow a different path to the output sensors. Nevertheless, for the Mach number range tested, the disturbance appears to follow the same path through the plant as the control input.

Recall that the input sensitivity was defined to aid in understanding the origins of spillover. Since the control objective is disturbance rejection, it is desired that $|S_i| < 1$ (negative log magnitude) over all frequencies. However, the Bode integral constraint places certain requirements on the sensitivity. Specifically, for a discrete data system with an asymptotically stable open-loop transfer function, $\mathbf{HP}$, the Bode integral constraint is:[35]

$$\int_0^\pi \log\left(|S_i\left(e^{j\omega}\right)|\right) d\omega = 0. \tag{20}$$

The immediate consequence of Eq. 20 is negative values of the log sensitivity in one frequency band must necessarily be balanced by positive values in another frequency band. The result is spillover and the current performance data clearly reflect this integral constraint.

It is important to consider whether the constraints imposed by the Bode integral can be overcome and therefore achieve arbitrary levels of broadband reduction. Hong and Bernstein[34] have shown that there are specific conditions under which a zero-spillover controller can be designed. One condition is that the disturbance and the control input be noncolocated. If they are colocated, then spillover is unavoidable. Since the present performance data suggest that the disturbance and control input are indeed colocated, spillover cannot be avoided. This is unfortunate since, from the standpoint of minimal control input energy, the cavity leading edge is an ideal place for actuation. From a controls perspective, however, it does not appear to be an optimal place to achieve *broadband* disturbance rejection.

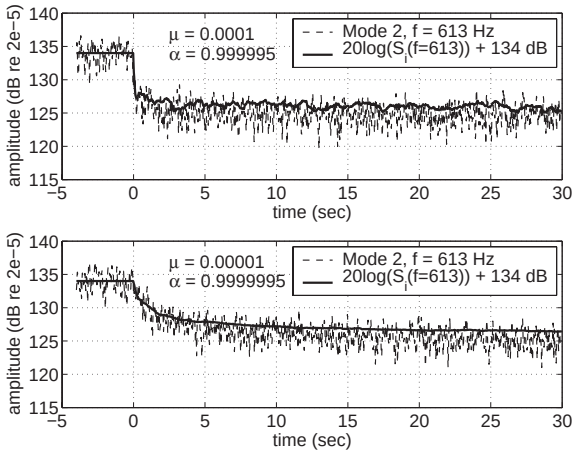

Fig. 8 Time evolution of Rossiter mode 2 amplitude for two adaptive rates. Controller was turned on at $t = 0$. The log magnitude of the input sensitivity at $f = 613$ Hz is plotted for comparison. $M_\infty = 0.275$.

Transient Behavior of the Algorithm

The transient behavior of the algorithm was examined through measurement of unsteady pressures and controller coefficients while the control algorithm was adapting. Unsteady pressure time series were collected in a pre/post-triggered mode, where the trigger condition was control on. The adaptive controller coefficients were also sampled at every 100th time step. For each test condition, 10 triggered data sets were acquired. The Short-Time Fourier Transform (STFT), which provides a measure of time evolution in the frequency spectrum, was then used to process the time-series data. The time and frequency resolution of the STFT was 13 $msec$ and 7.8 Hz, respectively. The STFT was block averaged over the 10 triggered data sets to reduce the random uncertainty in the estimate.

An example of the results is shown in Fig. 8. Here the amplitude of the STFT at the frequency of Rossiter mode 2 (613 Hz) for $M_\infty = 0.275$ and two adaptive rates ($\mu = 0.0001$, 0.00001) is plotted. The controller coefficients were initialized to zero and the algorithm was started at $t = 0$. Prior to control, the mode amplitude was ~ 134 dB. Once the control algorithm was started, the Rossiter mode amplitude decreased to a level of ~ 125 dB in the mean. For the larger adaptive rate, $\mu = 0.0001$, the Rossiter mode is suppressed within 2 seconds, while for the order-of-magnitude smaller adaptive rate, $\mu = 0.00001$, it takes an order-of-magnitude longer to reach a steady-state level of suppression. Although the adaptive rates are different, the same level of suppression is achieved, provided the leakage factor, α, is adjusted accordingly.

Using the sampled controller coefficients and the open-loop plant model, the input sensitivity at $f = 613$ Hz was computed for every 100th time step. This was performed for each of the 10 data sets and then block averaged. The results are shown in Fig. 8, where

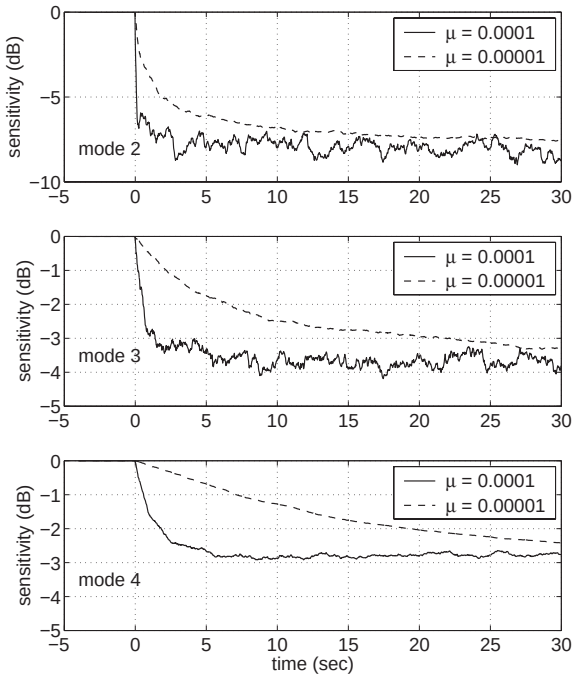

Fig. 9 Time evolution of input sensitivity for Rossiter modes 2, 3, and 4 and two adaptive rates. $M_\infty = 0.275$**.**

the log magnitude of the input sensitivity was shifted by 134 *dB* for comparison to the STFT results. Like the measured mode amplitude, the input sensitivity also reaches a steady state level. This occurs because the controller transfer function converges to a steady state. The convergence of the controller transfer function to a steady state suggests that adaptation can be stopped after some time to freeze the controller coefficients with no degradation in performance. Pressure spectra measured with a fixed set of converged controller coefficients confirmed this.

The input sensitivity closely matches the trend of the measured mode amplitude with time and therefore, it can be used to study the performance at other Rossiter frequencies. In Fig. 9, the input sensitivity at Rossiter modes 2, 3, and 4 for the $M_\infty = 0.275$ case is plotted for two adaptive rates. The plot demonstrates that the different Rossiter modes are suppressed at different convergence rates. The dominant mode is suppressed first, followed by the second largest mode, and so on. Nevertheless, given sufficient time, all Rossiter modes reach a steady-state level of suppression for a fixed Mach number.

The agreement between the transient performance data and the calculated input sensitivity in Fig. 8 supports treating the cavity dynamics as linear and time-invariant for a fixed Mach number. To test this hypothesis, it should be possible to design a GPC control law offline, using only the identified open-loop model, that yields similar performance to the adaptive GPC algorithm. Methods for computing the GPC gains offline can be found in several references.[19,20,22,23] Con-

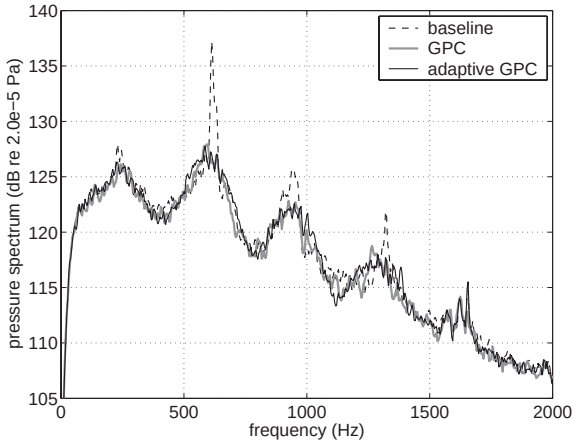

a) Baseline and controlled pressure spectra measured at rear-floor sensor for GPC and adaptive GPC. $M_\infty = 0.275$.

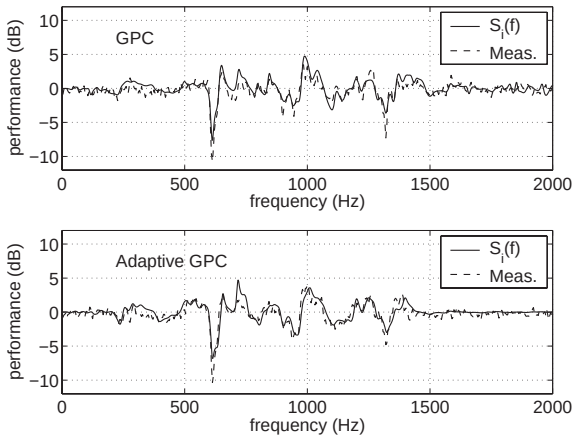

b) Comparison of measured performance and input sensitivity for GPC and adaptive GPC. $M_\infty = 0.275$.

Fig. 10 Comparison of GPC and adaptive GPC control results.

trol laws were designed offline for each Mach number tested and then compared to the adaptive GPC results. An example is shown in Fig. 10 for $M_\infty = 0.275$. The pressure spectra, measured performance, and input sensitivity for the GPC designed offline and the adaptive GPC are in close agreement. This was found to be true at the other Mach numbers tested.

Adaptation to Changing Mach Number

The adaptive GPC algorithm presented in this paper requires an estimate of the pulse response sequence of the open-loop plant. For a fixed Mach number, the results of the previous section indicate that the pulse response sequence can be determined offline from open-loop, input-output data and then subsequently used in the real-time control algorithm. If the Mach number changes, however, the open-loop dynamics change. Then, the open-loop dynamics will have to be identified with a recursive algorithm. This has not yet been implemented in our experimental program. It is still of interest to consider the robustness

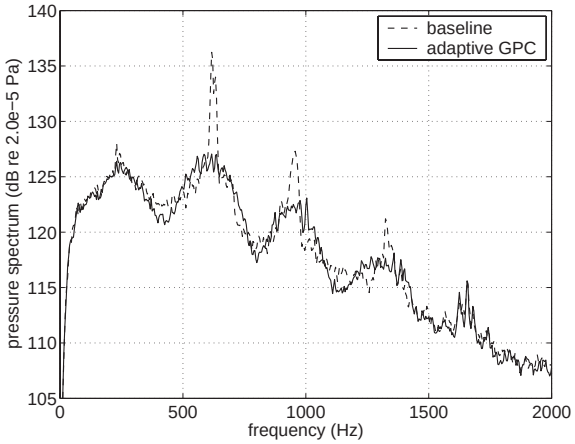

a) Baseline and adaptive GPC controlled pressure spectra measured at rear-floor sensor. $M_\infty = 0.28$.

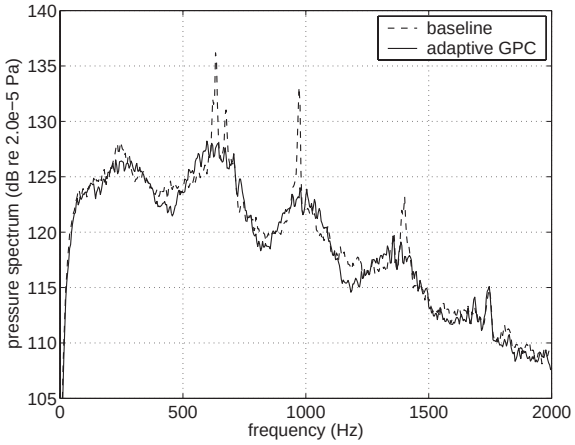

b) Baseline and adaptive GPC controlled pressure spectra measured at rear-floor sensor. $M_\infty = 0.29$.

Fig. 11 GPC and adaptive GPC control performance as freestream Mach number is increased. System identification was performed at $M_\infty = 0.275$.

of the adaptive algorithm to changes in the freestream Mach number without re-identification of the system. To that end, system identification was performed at $M_\infty = 0.275$. The control algorithm was then run at that Mach number and the controller was allowed to converge. The Mach number was then slowly increased to 0.28, while the controller continued to run, and time-series data were collected. Then, the Mach number was increased to 0.29 and data were again collected. Beyond this Mach number, a stable controller could not be maintained.

Baseline and controlled pressure spectra measured at the rear-floor sensor for $M_\infty = 0.28$ and 0.29 are shown in Fig. 11. For this small change in Mach number ($\sim$ 9 %) the controller is observed to maintain suppression in the first four Rossiter modes. Previous authors[36] have shown that for gradient descent algorithms where the gradient is filtered by a plant model, the condition for stability of convergence is that the ratio of the plant model to the true plant must be

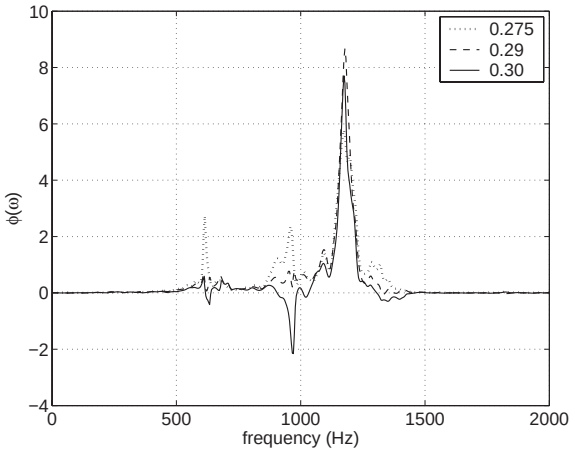

Fig. 12 Real part of the product in Eq. 21 for the path from rear error sensor at three Mach numbers.

strictly positive real. For the current application, this condition can be written

$$\phi(\omega) = \Re\left[\hat{G}_{0.275}(j\omega)G^\star_M(j\omega)\right] > 0 \quad \forall\omega, \qquad (21)$$

where $G^\star_M(j\omega)$ denotes the complex conjugate of the true plant from actuator to error sensors at the Mach number M, and $\hat{G}_{0.275}(j\omega)$ denotes the transfer function model for $M_\infty = 0.275$, which was the model used in the gradient update equation.

Although Eq. 21 requires knowledge of the true plant transfer function at each Mach number, an approximation to the condition in that equation can be obtained by using identified models of the plant at each Mach number. Figure 12 shows the real part of the product in Eq. 21 for the path from actuator to rear error sensor at three Mach numbers. At $M_\infty = 0.275$ and 0.29 the real part is greater than zero across the entire frequency range, indicating convergence should be stable. However, at $M_\infty = 0.30$, the real part is less than zero just above 600 *Hz* and just below 1000 *Hz*. These results thus confirm the experimental observations.

Conclusions

An adaptive generalized predictive control algorithm was formulated and applied to the cavity flow-tone problem. The algorithm employs gradient descent to update the GPC coefficients at each time step. Past input-output data and an estimate of the open-loop pulse response sequence are needed to implement the algorithm for application at fixed Mach numbers.

The adaptive control algorithm demonstrated multiple Rossiter mode suppression at fixed Mach numbers ranging from 0.275 to 0.38. For these Mach numbers, the controller coefficients were found to converge to a steady-state level. This implies that controller adaptation can be turned off at some point with no degradation in performance.

An input sensitivity transfer function was defined and shown to provide a useful measure of controller performance. The close agreement between the input sensitivity and a measure of output disturbance rejection suggests that the primary disturbance path is through the plant (cavity dynamics) from the input (cavity leading edge). This, in turn, suggests colocation of the control input and disturbance and therefore, arbitrary broadband pressure reduction is not possible with the present arrangement of sensors and actuators. Only the tonal components of the unsteady pressure fluctuations can be suppressed.

In the development of the adaptive control algorithm, the cavity dynamics were treated as linear and time-invariant (LTI) at a fixed Mach number. In that case, it is expected that the adaptive controller will converge to a steady state. It also follows that a GPC law designed offline using standard methods should yield similar performance to the adaptive controller. The experimental data lend support to the LTI treatment, since both expectations are displayed.

Finally, the adaptive control algorithm was applied to the cavity problem as the freestream Mach number was varied. The algorithm was able to maintain suppression of multiple cavity tones over a modest change in Mach number (0.275 to 0.29). Beyond this range, stable operation of the control algorithm was not possible. This limitation was the result of using a fixed plant model in the algorithm. To extend adaptation to higher Mach numbers, the system dynamics must be re-identified.

Future work should consider alternative placements of actuators and sensors. One possible arrangement would utilize actuation at both the leading and trailing edges of the cavity. Measurement sensors in the cavity shear layer may also be useful since then, a disturbance signal that is time advanced from actuation at the trailing-edge would be available. This feedforward type of arrangement may greatly enhance the control performance, particularly in regard to broadband disturbance rejection.

References

[1]Shaw, L. L. and Shimovetz, R. M., "Weapons bay acoustic environment," AGARD-CP-549, Sept. 1994.

[2]Williams, D. R., Fabris, D., Iwanski, K., and Morrow, J., "Closed-loop control in cavities with unsteady bleed forcing," AIAA Paper 2000-0470, Jan. 2000.

[3]Williams, D. R., Fabris, D., and Morrow, J., "Experiments on controlling multiple acoustic modes in cavities," AIAA Paper 2000-1903, June 2000.

[4]Kegerise, M. A., Cattafesta, L. N., and Ha, C., "Adaptive identification and control of flow-induced cavity oscillations," AIAA Paper 2002–3158, June 2002.

[5]Cabell, R. H., Kegerise, M. A., Cox, D. E., and Gibbs, G. P., "Experimental feedback control of flow induced cavity tones," AIAA Paper 2002–2497, June 2002.

[6]Cattafesta, L. N., Garg, S., Choudhari, M., and Li, F., "Active control of flow-induced cavity resonance," AIAA Paper 1997–1804, June 1997.

[7]Williams, D. R. and Morrow, J., "Adaptive control of multiple acoustic modes in cavities," AIAA Paper 2001–2769, June 2001.

[8]Cattafesta, L. N., Shukla, D., Garg, S., and Ross, J. A., "Development of an adaptive weapons-bay suppression system," AIAA Paper 99–1901, June 1999.

[9]Cattafesta, L. N., Williams, D. R., Rowley, C. W., and Alvi, F. S., "Review of active control of flow-induced cavity resonance," AIAA Paper 2003–3567, June 2003.

[10]Pillarisetti, A. and Cattafesta, L. N., "Adaptive identification of fluid-dynamic systems," AIAA Paper 2001–2978, June 2001.

[11]Rossiter, J. E., "Wind tunnel experiments on the flow over rectangular cavities at subsonic and transonic speeds," RAE Tech. Rep. 64037, Oct. 1964.

[12]Cattafesta, L. N., Garg, S., Kegerise, M. A., and Jones, G.S., "Experiments on compressible flow-induced cavity oscillations," AIAA Paper 98–2912, June 1998.

[13]Kegerise, M. A., Spina, E. F., Garg, S., and Cattafesta, L. N., "Mode-switching and nonlinear effects in compressible flow over a cavity," *Physics of Fluids*, Accepted for publication, 2003.

[14]Astrom, K. J. and Wittenmark, B. , *Adaptive Control*, Addison-Wesley, Reading, MA, 1995.

[15]Juang, J., *Applied System Identification*, Prentice-Hall, Englewood Cliffs, NJ, 1994.

[16]Ljung, L., *System Identification: Theory for the User*, Prentice-Hall, Upper Saddle River, NJ, 1999.

[17]Juang, J., Horta, L. G., and Phan, M., "System/observer/controller identification toolbox," NASA TM–107566, Feb. 1992.

[18]Juang, J. and Phan, M., "Deadbeat predictive controllers," NASA TM–112862, May 1997.

[19]Juang, J. and Eure, K. W., "Predictive feedback and feedforward control for systems with unknown disturbances," NASA TM–1998–208744, Dec. 1998.

[20]Clarke, D. W., Mohtadi, C., and Tuffs, P. S., "Generalized predictive control – Part I. The basic algorithm," *Automatica*, Vol. 23, No. 2, 1987, pp. 137–148.

[21]Clarke, D. W., Mohtadi, C., and Tuffs, P. S., "Generalized predictive control – Part II. Extensions and interpretations," *Automatica*, Vol. 23, No. 2, 1987, pp. 149–160.

[22]Eure, K. W. and Juang, J., "Broadband noise control using predictive techniques," NASA TM–110320, Jan. 1997.

[23]Phan, M. Q., Lim, R. K., and Longman, R. W., "Unifying input-output and state-space perspectives of predictive control," MAE Tech. Report No. 3044, Princeton University, Princeton, NJ, 1998.

[24]Haykin, S., *Adaptive Filter Theory*, Prentice Hall, Upper Saddle River, NJ, 1996.

[25]Widrow, B. and Stearns, S. D., *Adaptive Signal Processing*, Prentice Hall, Upper Saddle River, NJ, 1985.

[26]Darlington, P., "Performance surfaces of minimum effort estimators and controllers," *IEEE Trans. on Signal Processing*, Vol. 43, No. 2, 1995, pp. 536–539.

[27]Elliott, S. J., *Signal Processing for Acitve Control*, Academic Press, San Diego, CA, 2001.

[28]Cattafesta, L. N., Garg, S., and Shukla, D., "Development of Piezoelectric Actuators for Active Flow Control," *AIAA Journal*, Vol. 39, No. 8, Aug. 2001, pp. 1562–1568.

[29]Mathew, J. , *A Theoretical and Experimental Study of Piezoelectric Unimorph Actuators for Active Flow Control*, M. S. Thesis, University of Florida, June 2002.

[30]Schaeffler, N. W., Hepner, T. E., Jones, G. S., and Kegerise, M. A., "Overview of active flow control actuator development at NASA Langley Research Center," AIAA Paper 2002-3159, June 2002.

[31]Heller, H. H., Holmes, D. G., and Covert, E. E., "Flow-induced pressure oscillations in shallow cavities," *J. Sound Vib.,* Vol. 18, No. 4, 1971, pp. 545–553.

[32]Rowley, C. W., Williams, D. R., Colonius, T., Murray, R. M., MacMartin, D. G., and Fabris, D., "Model-based control of cavity oscillations Part II: System identification and analysis," AIAA Paper 2002-0972, Jan. 2002.

[33]Rowley, C. W. and Williams, D. R., "Control of forced and self-sustained oscillations in the flow past a cavity," AIAA Paper 2003–0008, Jan. 2003.

[34]Hong, J. and Bernstein, D. S., "Bode integral contraints, colocation, and spillover in active noise and vibration control," *IEEE Trans. on Control Systems Tech.*, Vol. 6, No. 1, 1998, pp. 111–120.

[35]Franklin, G. F., Powell, J. D., and Workman, M. L., *Digital Control of Dynamic Systems*, Addison-Wesley, Menlo Park, CA, 1998.

[36]Ren, W. and Kumar, P. R., "Adaptive active noise control:structures, algorithms, and convergence analysis," *Proceedings of Inter–Noise 89*, 1989, pp. 435–440.

Appendix

In this section, the performance measure defined in Eq. 18 is shown to be equal to the input sensitivity for the SIMO model shown in Fig. 7. To that end, an expression for the closed-loop response of the SIMO system must first be formed. The cavity flow is considered to be a single-input/multiple-output system described by:

$$\mathbf{y}(f) = \mathbf{G}(f)v(f), \tag{22}$$

where $\mathbf{G}(f)$ is an $m \times 1$ frequency response function matrix of the cavity flow. The controller is a multiple-input/single-output system described by:

$$u(f) = \mathbf{H}(f)\mathbf{y}(f) \tag{23}$$

where $\mathbf{H}(f)$ is a $1 \times m$ frequency response function matrix of the controller. The input to the cavity flow is given by:

$$v(f) = w(f) + G_a(f)u(f). \tag{24}$$

Substituting Eqs. 23 and 24 into Eq. 22 yields:

$$\mathbf{y} = \mathbf{G}w + \mathbf{G}G_a\mathbf{H}\mathbf{y}, \tag{25}$$

where the dependence on frequency, f, is understood. Solving this expression for $\mathbf{y}$ gives the closed-loop response:

$$\mathbf{y} = \left[\mathbf{I} - \mathbf{G}G_a\mathbf{H}\right]^{-1}\mathbf{G}w. \tag{26}$$

Using the matrix inversion lemma:

$$\left[\mathbf{A} + \mathbf{BCD}\right]^{-1} = \mathbf{A}^{-1} - \mathbf{A}^{-1}\mathbf{B}\left[\mathbf{C}^{-1} + \mathbf{D}\mathbf{A}^{-1}\mathbf{B}\right]^{-1}\mathbf{D}\mathbf{A}^{-1}, \tag{27}$$

the matrix inverse in Eq. 26 can be written as:

$$\mathbf{I} + \mathbf{G}\left(\frac{1}{G_a} - \mathbf{H}\mathbf{G}\right)^{-1}\mathbf{H} \tag{28}$$

or

$$\mathbf{I} + \frac{\mathbf{G}G_a\mathbf{H}}{1 - \mathbf{H}\mathbf{G}G_a}. \tag{29}$$

Substituting this expression into Eq. 26 gives:

$$\mathbf{y} = \frac{\mathbf{G} - \mathbf{H}\mathbf{G}G_a\mathbf{G} + \mathbf{G}G_a\mathbf{H}\mathbf{G}}{1 - \mathbf{H}\mathbf{G}G_a}w. \tag{30}$$

Since $\mathbf{HG}$ and G_a are scalar transfer functions, Eq. 30 can be rewritten as:

$$\mathbf{y} = \frac{\mathbf{G} - \mathbf{G}G_a\mathbf{H}\mathbf{G} + \mathbf{G}G_a\mathbf{H}\mathbf{G}}{1 - \mathbf{H}\mathbf{G}G_a}w \tag{31}$$

and therefore,

$$\mathbf{y} = \frac{\mathbf{G}}{1 - \mathbf{H}\mathbf{G}G_a}w. \tag{32}$$

The input sensitivity for the SIMO system is given by:

$$S_i = \frac{1}{1 - \mathbf{H}\mathbf{G}G_a} \tag{33}$$

Using this definition, the closed-loop response for the model system can be written as:

$$\mathbf{y}_{cl} = S_i\mathbf{G}w. \tag{34}$$

where the subscript was added to denote the closed-loop response.

In the absence of feedback control, the open-loop response of the cavity flow is described by:

$$\mathbf{y}_{ol} = \mathbf{G}w. \tag{35}$$

Recall the performance measure defined earlier:

$$\frac{\|\mathbf{y}_{cl}(f)\|_2}{\|\mathbf{y}_{ol}(f)\|_2} = \frac{\sqrt{\mathbf{y}_{cl}^T\mathbf{y}_{cl}}}{\sqrt{\mathbf{y}_{ol}^T\mathbf{y}_{ol}}}. \tag{36}$$

Substituting Eqs. 34 and 35 into 36 gives:

$$\frac{\|\mathbf{y}_{cl}(f)\|_2}{\|\mathbf{y}_{ol}(f)\|_2} = \frac{\sqrt{\mathbf{G}^T\mathbf{G}}}{\sqrt{\mathbf{G}^T\mathbf{G}}}S_i = S_i. \tag{37}$$

Therefore, for this special case of a single control input, a single disturbance input, and multiple output sensors, the input sensitivity is equal to the performance measure.